

PUBLISHED VERSION

Nafisa Zohora, Ahmad Esmailzadeh Kandjani, Antony Orth, Hannah M. Brown, Mark R. Hutchinson and Brant C. Gibson

Fluorescence brightness and photostability of individual copper (I) oxide nanocubes

Scientific Reports, 2017; 7(1):16905-1-16905-8

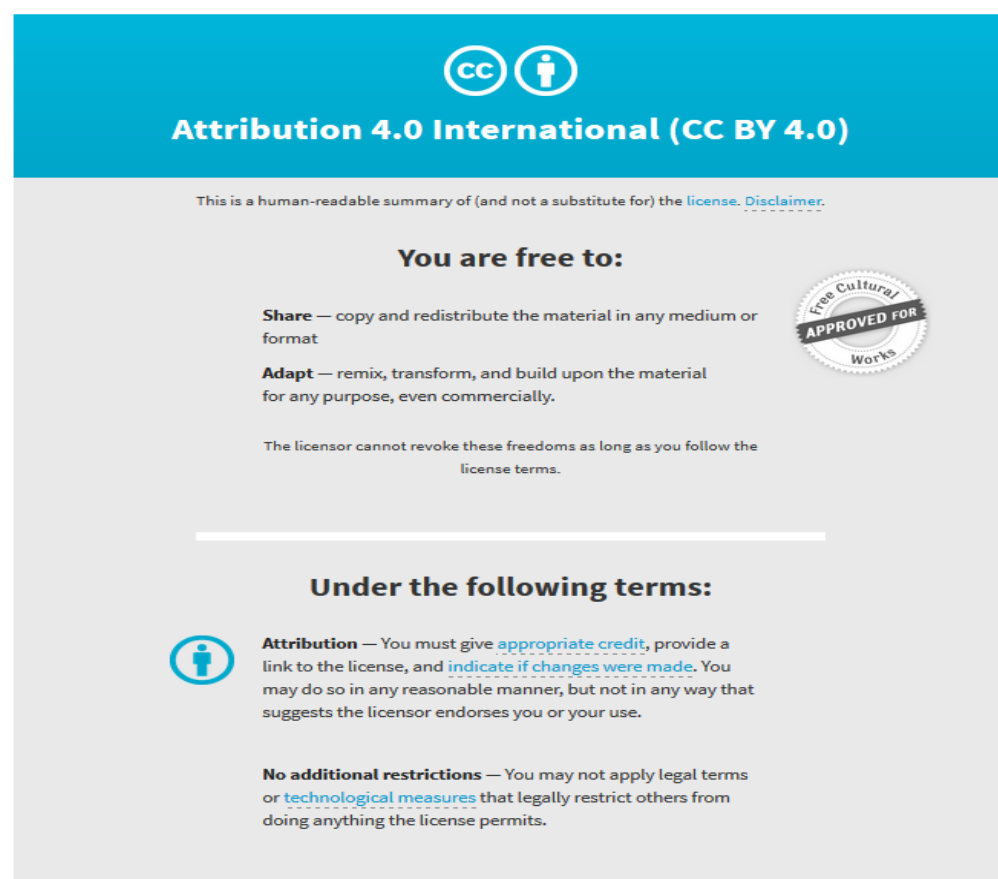
© The Author(s) 2017. Open Access This article is licensed under a Creative Commons Attribution 4.0 International License, which permits use, sharing, adaptation, distribution and reproduction in any medium or format, as long as you give appropriate credit to the original author(s) and the source, provide a link to the Creative Commons license, and indicate if changes were made. The images or other third party material in this article are included in the article's Creative Commons license, unless indicated otherwise in a credit line to the material. If material is not included in the article's Creative Commons license and your intended use is not permitted by statutory regulation or exceeds the permitted use, you will need to obtain permission directly from the copyright holder. To view a copy of this license, visit <http://creativecommons.org/licenses/by/4.0/>.

Originally published at:

<http://doi.org/10.1038/s41598-017-17295-0>

PERMISSIONS

<http://creativecommons.org/licenses/by/4.0/>



The image is a summary graphic for the Creative Commons Attribution 4.0 International License (CC BY 4.0). It features a blue header with the CC and BY icons and the text "Attribution 4.0 International (CC BY 4.0)". Below the header, it states "This is a human-readable summary of (and not a substitute for) the license. [Disclaimer.](#)". The main content is divided into two sections: "You are free to:" and "Under the following terms:". Under "You are free to:", it lists "Share" (copy and redistribute) and "Adapt" (remix, transform, and build upon), with a "Free Cultural Works APPROVED FOR Works" seal. Under "Under the following terms:", it lists "Attribution" (provide credit and link) and "No additional restrictions" (no legal terms or technological measures).

Attribution 4.0 International (CC BY 4.0)

This is a human-readable summary of (and not a substitute for) the [license](#). [Disclaimer.](#)

You are free to:

Share — copy and redistribute the material in any medium or format

Adapt — remix, transform, and build upon the material for any purpose, even commercially.

The licensor cannot revoke these freedoms as long as you follow the license terms.

Under the following terms:

Attribution — You must give [appropriate credit](#), provide a link to the license, and [indicate if changes were made](#). You may do so in any reasonable manner, but not in any way that suggests the licensor endorses you or your use.

No additional restrictions — You may not apply legal terms or [technological measures](#) that legally restrict others from doing anything the license permits.

1st of May

<http://hdl.handle.net/2440/110994>

SCIENTIFIC REPORTS

OPEN

Fluorescence brightness and photostability of individual copper (I) oxide nanocubes

Nafisa Zohora¹, Ahmad Esmailzadeh Kandjani², Antony Orth¹, Hannah M. Brown³, Mark R. Hutchinson⁴ & Brant C. Gibson¹

Conventional organic fluorophores lose their ability to fluoresce after repeated exposure to excitation light due to photobleaching. Therefore, research into emerging bright and photostable nanomaterials has become of great interest for a range of applications such as bio-imaging and tracking. Among these emerging fluorophores, metal oxide-based nanomaterials have attracted significant attention as a potential multifunctional material with photocatalytic and angiogenesis abilities in addition to fluorescence applications. However, most of these applications are highly dependent on size, morphology, and chemo-physical properties of individual particles. In this manuscript, we present a method to study the intrinsic optical characteristics of individual copper (I) oxide (Cu₂O) nanocubes. When excited at 520 nm using only 11 μW excitation power (1.7 W/cm²), individual nanocubes were observed to emit light with peak wavelengths ~760 nm which is conveniently within the near-infrared 1 (NIR1) biological window where tissue autofluorescence is minimal. Bright and photostable fluorescence was observed with intensities up to 487 K counts/s under constant illumination for at least 2 minutes with a brightness approximately four times higher than the autofluorescence from a fixed cumulus-oocyte complex. With near-IR emission, high fluorescence brightness, and outstanding photostability, Cu₂O nanocubes are attractive candidates for long-term fluorescent bioimaging applications.

Copper (I) oxide (Cu₂O) is a p-type semiconductor material with a direct bandgap 2.17 eV in bulk form^{1–5}. This semiconducting material has attracted much attention due to its exceptional properties which are possible in nano-sized particles. Various morphologies are possible such as nanocubes, nanospheres, nanorods and nano-octahedrons, as reported in the literature, synthesised via simple methods and low preparation costs^{1–12}. These approaches make this material suitable for scalable manufacturing and provide a competitive edge as an oxide semiconducting material. Copper (I) oxide shows a high absorption coefficient at around 438 nm in bulk and ensembles, has more than 10% energy conversion efficiency and a quantum yield of $6.6 \times 10^{-2}\%$ when excited at 360 nm and emission at 493 nm¹³ which makes this material a promising candidate for various photoelectronic applications, such as photovoltaic cells and photo-capacitors^{13,14}. Other areas of interest which explore the use of Cu₂O nanoparticles are in the fields of biological imaging¹⁵ and photocatalysis^{3,16}. As an example, Qi *et al.* have used Cu₂O nanoparticles for light scattering imaging of living cells and as a probe for conformation of proteins¹⁵, where they report changes in circular dichroism of specific proteins such as prion (PrPC) and bovine serum albumin (BSA) due to the introduction of Cu₂O nanoparticles. It has been shown that the optical and electrical properties of Cu₂O semiconductors are highly dependent on their morphology and the growth of the crystal facets of Cu₂O nanoparticles^{12,17}. Among the various morphologies of nano-copper (I) oxides, nanocubic morphologies have attracted great attention due to their well-defined cubic structure and shape homogeneity. Ensembles of Cu₂O nanoparticles have also been shown to have an intraband photoemission due to oxygen vacancies which give rise to 750 nm emission with 532 nm excitation¹⁸. The emission at 750 nm makes this nanoparticle a good

¹ARC Centre of Excellence for Nanoscale BioPhotonics, School of Science, RMIT University, Melbourne, VIC 3001, Australia. ²Centre for Advanced Materials and Industrial Chemistry, School of Science, RMIT University, Melbourne, VIC 3001, Australia. ³ARC Centre of Excellence for Nanoscale BioPhotonics, Robinson Research Institute, Adelaide Medical School, The University of Adelaide, Adelaide, SA 5005, Australia. ⁴ARC Centre of Excellence for Nanoscale BioPhotonics, Adelaide Medical School, University of Adelaide, Adelaide, SA 5005, Australia. Correspondence and requests for materials should be addressed to N.Z. (email: nafisa.zohora@rmit.edu.au) or B.C.G. (email: brant.gibson@rmit.edu.au)

candidate for bioimaging applications as the emission lies within the NIR1 biological window¹⁹. However, up until now, the optical fluorescent properties of individual, isolated Cu₂O nanoparticles have not been studied.

The emerging area of biophotonics requires the development of intrinsically bright and photostable luminescent nanoproboscopes. Our approach in this paper is to explore the optical properties of individual and isolated cubic Cu₂O nanoparticles, which are monodisperse in size. Previous characterisation and analytical studies that have been reported in the literature for Cu₂O nanoparticles have focused on ensemble colloid solutions or bulk materials that are widely dispersed in size and morphology, resulting in cumulative measurements^{20,21}. Collecting bright and stable emission from fluorescent organic dyes or nanoparticles using low laser excitation is essential when these fluorophores are used for biological imaging. Biological samples are sophisticated and highly responsive to laser irradiation as high laser power coagulates proteins of tissues, thus it can destroy a sample²². Hence, it is desirable for a fluorescent nanoparticle to exhibit bright emission, above that of any surrounding background fluorescence, with minimal optical excitation. In this research, we have examined individual Cu₂O nanocubes using silicon wafers which have been milled using a focused ion beam to create registration markers²³. The marked substrates are visible in both a confocal microscope and scanning electron microscope (SEM) and enable the characterisation of isolated nanocubes without interaction from adjacent particles. We now present the first study of the optical fluorescent properties of individual Cu₂O nanocubes, compare their performance against existing commercially available fluorescent materials, focusing on the intrinsic brightness and photostability of the material for bioimaging applications.

Experimental

Chemicals for Cu₂O synthesis. Copper (II) sulphate (CuSO₄), Sodium dodecyl sulphate (C₁₂H₂₅NaO₄S), (+)-Sodium L- ascorbate (C₆H₇NaO₆) and Sodium hydroxide (NaOH) were used in the synthesis of Cu₂O nanocubes. All chemicals were obtained from Sigma-Aldrich and used as received. The water used was double distilled de-ionized Milli-Q water 18.2 MΩ.cm.

Chemicals used for cumulus-oocyte complex preparation. αMEM supplemented with bovine serum albumin (BSA; ICPbio, Glenfield, New Zealand), Recombinant human follicle-stimulating hormone (50 mIU/ml; Organon, Oss, The Netherlands), equine chorionic gonadotropin (eCG; Folligon, Intervet, Boxmeer, The Netherlands).

Cu₂O nanoparticle synthesis. A seed-mediated growth method¹ was used to synthesise Cu₂O nanocubes which were tailored to increase the yield of Cu₂O nanocubes compared to the in the published synthesis process. A solution containing 1 mM of CuSO₄ and 33 mM Sodium dodecyl sulphate (SDS) was prepared and 30 ml of the prepared mixture was transferred to a round bottle flask (bottle A) followed by the addition of 750 μL of 0.2 M (+)-Sodium L-ascorbate. The solution was vigorously shaken for 5 seconds followed by the addition of 1 M NaOH and shaken another 5 seconds. Then, 20 mL of solution from bottle A was transferred to another round bottle flask (bottle B) with 180 ml of the starting solution and kept in constant shaking for 10 seconds. Then, 5 mL of 0.2 M (+)-Sodium L- ascorbate was added to bottle B and shaken for 5 seconds. Afterwards, 10 mL of 1 M NaOH was added to bottle B and then shaken for another 5 seconds. Sample B was kept standing for one hour. The synthesised Cu₂O nanocubes were centrifuged at 5000 rpm and washed three times for ten minutes each and redispersed in 10 ml ethanol

Characterization. The morphological studies of synthesised Cu₂O nanocubes were carried out with FEI Verios 460 L scanning electron microscope using 10 kV and 0.8 nA. The structural characteristics of the synthesised materials were studied using Bruker D8 Discover microdiffraction system which has general area detector diffraction system and the Cu-Kα radiation source. The oxidation state studies of the prepared samples were studied using Thermo K-Alpha instrument at a pressure better than ~10⁻⁸ Torr. The core binding energies of the elements were aligned at 285 eV for adventitious C1s core level energy. Si substrates were marked using focused ion beam milling with a FEI Scios FIB-SEM. Each marked area on the silicon has a size of 286 μm × 286 μm with an etched depth of 1 μm. A beam current 3 nA at 30 KV was used for 516 seconds with tilt 52° to mill each substrate. Fluorescence confocal images were taken using a 6 ps pulsed Fianium SuperChrome laser source, at a repetition rate of 40 MHz, with a centre wavelength of 520 nm and a full width at half maximum (FWHM) of 10 nm. The imaging was performed using a 532 nm dichroic mirror, 532 nm long pass filter, 532 nm short pass filter and a 100 × 0.9 NA objective lens.

Tracking individual particles. Individual Cu₂O nanocubes were studied using a marked silicon substrate²³ which was milled with focused ion beam (FIB). The marked Si substrate was drop cast with one drop of the sample. A low magnification SEM image of the deposited, marked substrate was taken to locate regions of isolated particles. Afterwards, the individual particles have been numbered (P1 to P19) and then optical data have been collected the marked individual and isolated Cu₂O particles.

Cumulus-oocyte complex (COC) sample preparation. All animal work was approved by the University of Adelaide Animal Ethics Committee. Female mice were administered 5 IU equine chorionic gonadotropin (i.p.) (eCG; Folligon, Intervet, Boxmeer, The Netherlands). 46 hours post-eCG injection, ovaries were collected and COCs liberated from antral follicles. COCs were then placed in maturation medium and matured for 16 hours in a volume of 50 μl medium/COC at 37 °C under paraffin oil, in humidified air comprised of 20% O₂, 6% CO₂ and N₂ balance. Following maturation, COCs were fixed in 4% paraformaldehyde in phosphate-buffered saline (PBS) and mounted on glass slides using DAKO Fluorescence Mounting Medium (Dako, NSW, Australia). Cu₂O nanocubes were transferred to water and were drop cast on the biological sample to study the intensity variation between fixed biological sample and Cu₂O nanocubes.

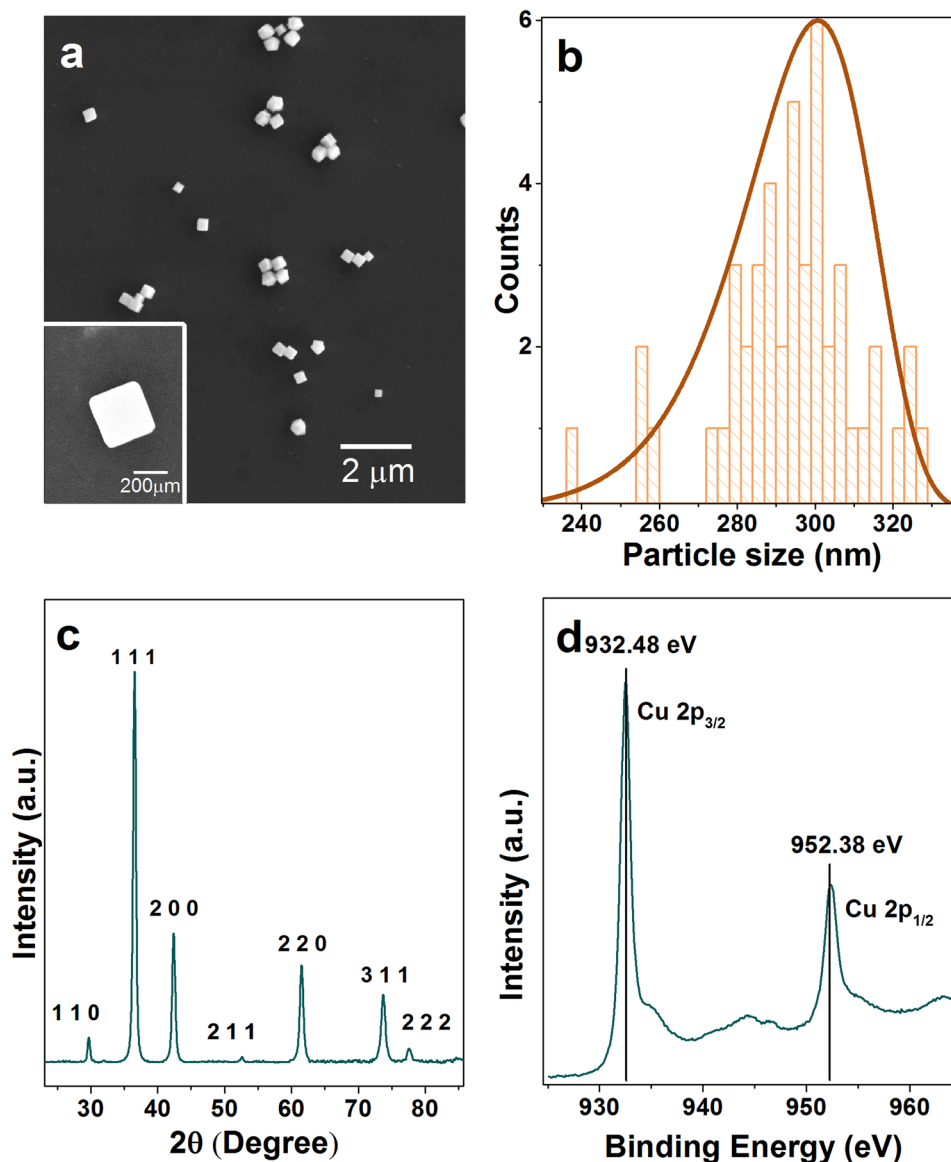


Figure 1. (a) SEM image of Cu_2O nanocubes showing cubic morphology with an individual isolated nanocube shown in the inset. (b) Size distribution of each of the Cu_2O nanocubes analysed with a peak side length of 293 ± 18 nm. (c) XRD pattern of Cu_2O nanocubes where (111) crystal facet has the highest intensity. (d) XPS Cu2p scan showing Cu 2p $3/2$ peak at 932.5 eV and Cu 2p $1/2$ peak at 952.4 eV with satellite peaks at 943.8 eV and 946.3 eV representing the formation of Cu_2O with small amounts of the CuO impurities based on the satellite peaks at 944.3 eV and 963.1 eV.

Results and Discussion

Cu_2O nanocubes were synthesised using a previously reported seed-mediated approach^{1,3}. In this synthesis method, sodium ascorbate acts as a reducing agent, sodium dodecyl sulphate as a capping agent, and sodium hydroxide was used to form $\text{Cu}(\text{OH})_4^{2-}$, which was then reduced to produce Cu_2O seeds. These seeds produce cubic Cu_2O nanoparticles after Ostwald ripening and surface reconstruction¹. SEM images confirmed the truncated cubic shape and smooth surfaces of the particles (Fig. 1a). The average lengths of cubic Cu_2O are 293 ± 18 nm along one side (Fig. 1b). The X-ray powder diffraction (XRD) pattern of the sample shows the formation of the face-centered cubic lattice Cu_2O (JCPDF No. 78–2076) (Fig. 1c). To further confirm the formation of Cu_2O , oxidation state analysis was carried out using X-ray photoelectron spectroscopy (XPS) analysis. The low-resolution XPS survey spectrum (Figure S1) showed the presence of C1s, O1s, Cu2p, and Na1s peak, where C1s is related to the surface adsorbed adventitious carbon while the Na is related to the trace chemicals remaining from the starting materials. It showed that the core level of the Cu 2p $3/2$ has 932.5 eV and Cu 2p $1/2$ has 952.4 eV binding energy indicating the oxidation state of Cu(I) (Fig. 1d). Satellite peaks in CuO structures have higher intensities than Cu_2O structures. Also, the position of these satellite peaks is different in these two oxidation states. The satellite peaks appearing at 943.8 eV and 946.3 eV are related to Cu(I) while the presence of the peaks at

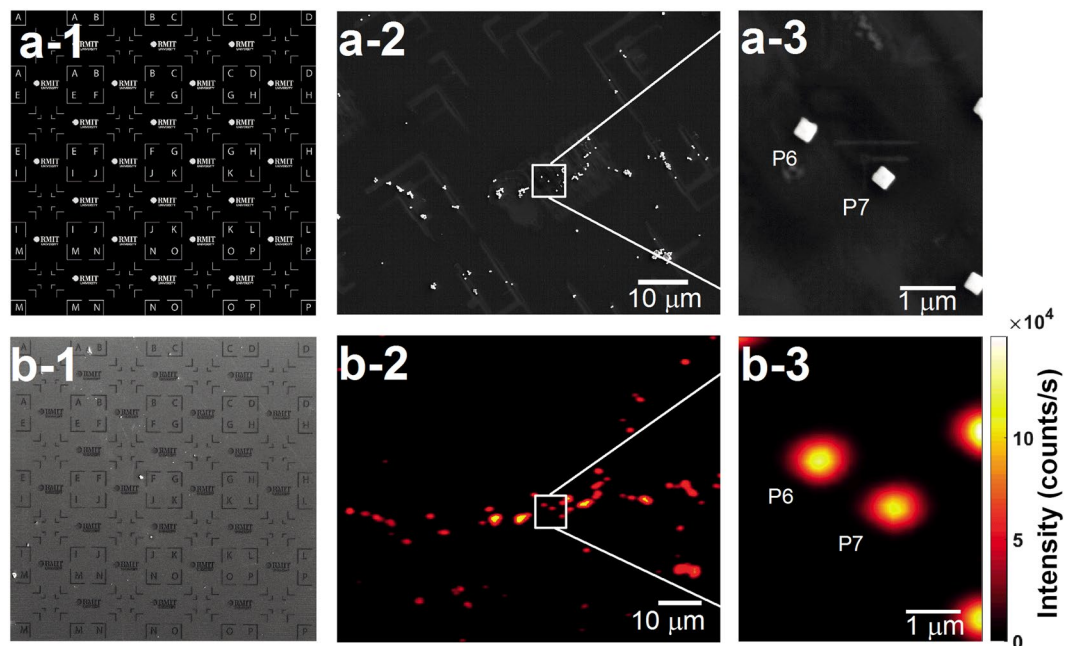


Figure 2. (a-1) Template of the registration marker which was milled on a silicon substrate using a focused ion beam (FIB) (b-1). SEM image of Cu_2O nanocubes dropped cast on a silicon substrate with registration markers to enable the location of the exact area of a certain isolated Cu_2O nanocube. (a-2) Low magnification SEM image of Cu_2O nanocubes. This type of image was taken of different areas of the substrate to select individual nanocubes P1 to p19. (a-3) High-resolution SEM image of the boxed region in (a-2) which was taken after acquiring the optical data to avoid the effect of the electron beam on the optical properties of the Cu_2O nanocubes. Particles P6 and P7 are shown as an example of two isolated nanocubes. (b-2) Confocal fluorescence image of the same field-of-view as in (a-2). (b-3) High-resolution confocal fluorescence image of the boxed region in (b-2) of particles P6 and P7.

944.3 eV and 963.1 eV relate to the existence of trace CuO impurities¹⁷. The XRD and XPS results indicate that the synthesised cubic structures are predominantly Cu_2O structures³. Other than the XRD and XPS analysis, the zeta potential of the particles was also measured yielding -17.4 ± 4.7 mV. The zeta potential information is valuable for future functionalizing of the nanocubes with additional materials for targeted biological imaging applications. This result also means that these Cu_2O nanocubes can increase the surface adsorption ability between nanocubes and charged molecules for biolabelling applications²⁴.

A template registration marker, shown in Fig 2a-1 was milled into a silicon substrate with a focused ion beam to enable the characterization of isolated Cu_2O nanocubes. This was followed by drop casting the synthesised nanocubes and drying under air (Fig. 2a-2). A low magnification scanning electron microscope (SEM) image was taken to locate regions of individual and isolated Cu_2O nanocubes (Figure 2a-2)²³. The marked silicon platform was used to locate and measure the optical properties of individual particles under a confocal microscope. To confirm the size, morphology, and isolation of particles, high-magnification SEM images were taken after all optical data was acquired from 19 individual nanocubes in order to minimise any effect of possible electron beam damage on their optical properties. Figure 2a-1 represents the template of the registration pattern which has been milled as shown in Fig. 2b-1. A SEM image of the nanocubes on the registered Si wafer is shown in Fig. 2a-2 at low magnification. As an example in Fig 2a-3, we show a high magnification SEM image of two typical individual nanocubes (particles number P6 and P7). Confocal fluorescence images for low and high magnifications are shown in Fig. 2b-2 and b-3, respectively. These images are collected using the same field-of-view as the SEM images shown in Fig. 2a-2 and a-3, respectively, to enable subsequent photostability and spectral measurements.

UV-visible absorbance spectrum of Cu_2O nanocubes in water was collected, which showed maximum absorbance appeared at 481 nm (Fig. 3a), in addition, the UV-Vis absorbance spectra near-IR absorbance at 750 nm which is well aligned with previously reported literatures^{4,3}. Fluorescence spectral data was collected from individual and isolated Cu_2O particles on the marked silicon substrate using 520 nm (2.38 eV) supercontinuum pulsed laser with 11 μW average excitation power (1.7 W/cm^2) at room temperature with an FWHM = 10 nm. This pump wavelength was chosen because visible light excitation is compatible with biological imaging¹⁹. Under these excitation conditions, the emission peak of individual Cu_2O nanocubes was centred around 754.6 ± 2 nm (Fig. 3b,c) which can be assigned to doubly charged oxygen vacancies (V_O)¹⁸ in the Cu_2O nanocube lattice. Having an emission at 754 nm makes this material a promising candidate for biological imaging as tissue absorption and autofluorescence are minimal in this emission range¹⁹. The peak in the distribution of full width at half-maximum (FWHM) emission is around 85 nm (Fig. 3d).

In addition to the emission wavelength, brightness and photostability are crucial factors for bioimaging applications. Brightness and photostability data were collected from the same isolated individual Cu_2O particles

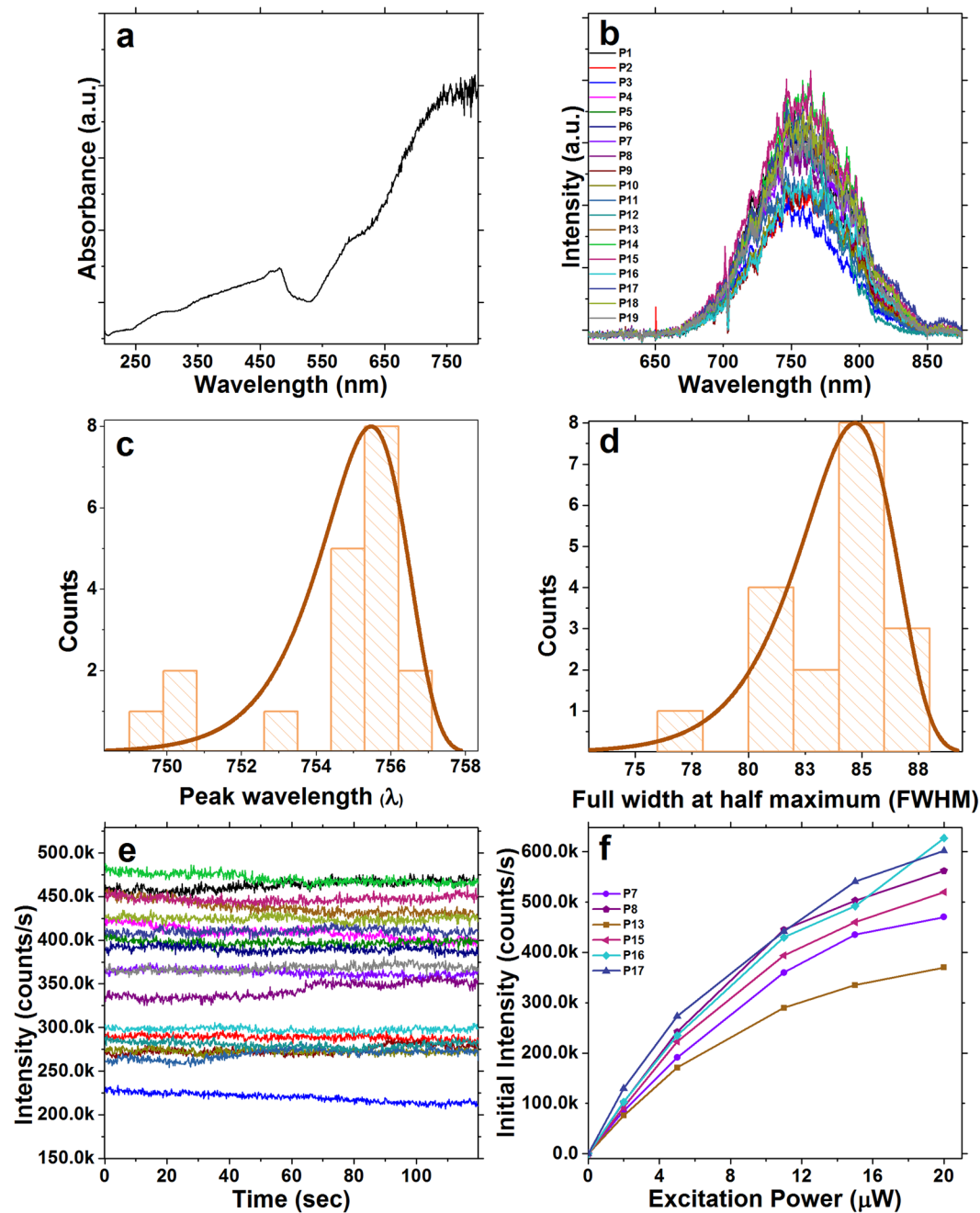


Figure 3. (a) UV-visible absorbance spectrum of Cu_2O nanocubes in water. (b) Fluorescence emission spectra of 19 individual Cu_2O nanocubes excited at 520 nm with a supercontinuum picosecond pulsed laser. (c) Emission peak wavelength distribution. The emission peak centered at 754.6 ± 2 nm which can be correlated to oxygen vacancy (V_o). This wavelength is well suited for biological imaging applications. (d) The peak in the distribution of full width at half-maximum (FWHM) emission is around 85 nm. (e) Fluorescence intensity of the same nanocubes as in (a) over a 120 second time period of continuous excitation with $11 \mu\text{W}$ time-averaged power at the sample from the supercontinuum pulsed laser. Emission intensities of these individual particles ranged between 226 k to 780 k counts/s. (f) Fluorescence emission intensity of 6 selected individual Cu_2O nanocubes under $2 \mu\text{W}$, $5 \mu\text{W}$, $11 \mu\text{W}$, $15 \mu\text{W}$ and $20 \mu\text{W}$ excitation power. The selected nanocubes in (f) are a subset, chosen for no particular reason, of those studied in (b) and (e). This result indicates that individual Cu_2O nanocubes have the ability to produce considerably bright emission while using low excitation powers.

(using 520 nm excitation wavelength with $11 \mu\text{W}$ average power with $\text{FWHM} = 10$ nm for 120 seconds), as shown in Fig. 3e. Emission counts ranged between 226 k and 780 k counts/s, and remained stable for a period of at least 120 seconds, indicating photostable characteristics of the Cu_2O nanocubes. It should be mentioned that the laser power used in this part of the research is considerably lower than that used for some biological imaging

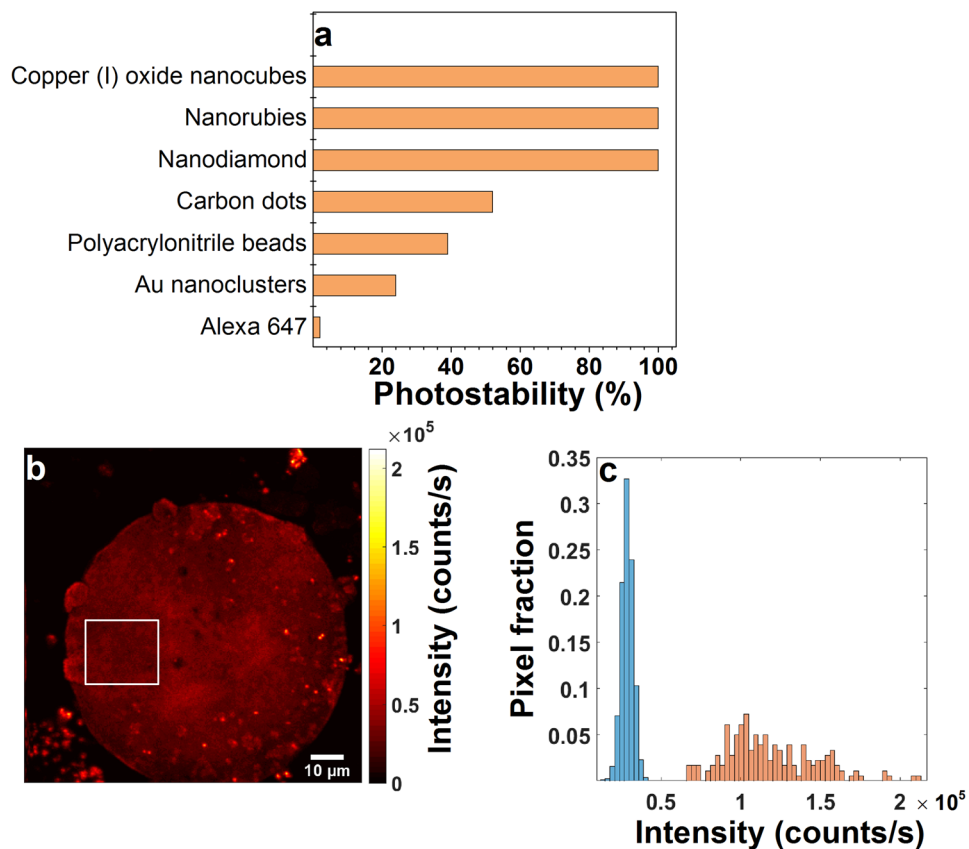


Figure 4. (a) Comparison of the photostability of Cu_2O nanocubes with commercial dyes and emerging fluorescent nanoparticles over a time period of 120 seconds (Table S1)1. The photostability of Cu_2O nanocubes are 98% higher than the widely used commercial Alexa 647 dye and 48% higher than carbon dots. Cu_2O nanocubes, nanorubies and nanodiamonds are showing 100% photostability over this time period. (b) Confocal fluorescence image of a mouse cumulus-oocyte complex with Cu_2O nanocubes. Bright dots are Cu_2O nanocubes. (c) Histogram showing the relative brightness of autofluorescence (blue bars) and Cu_2O nanocube fluorescence (orange bars). The autofluorescence histogram shows the distribution of pixel intensities within the boxed region in (b). The Cu_2O histogram shows the brightness distribution of 20 manually selected Cu_2O particles in (b). The Cu_2O nanocubes were observed to be approximately 4 times brighter than autofluorescence from the mouse cumulus-oocyte complex hence making them easily distinguishable.

applications²⁵. For example, Goetz, M., *et al.* reported confocal imaging during mini-laparoscopy where they used 715 μW average laser power with maximum power limited to 2000 μW ²⁶. Laser power ranged between 300 mW and 600 mW was used for histomorphologic imaging of brain tumours *in vivo*²⁷.

In addition, the relationship between excitation power and emission counts was studied for 6 individual Cu_2O particles using 5 excitation powers (Fig. 3f). This study shows that it is possible to observe counts ranging between 76k counts/s and 130k counts/s from a single Cu_2O nanocube using only 2 μW of excitation power with a pulsed laser. The intensity of emitted light was observed to increase with increasing excitation power (Fig. 3f). It is an important factor in bioimaging to use low power excitation lasers as there are reports indicating that higher laser power can damage biological samples²². The results showed that when a pulsed laser is used for imaging, saturation has not occurred over a range up to 20 μW laser excitation power. The intensity of the emission from individual Cu_2O with 20 μW laser excitation was ranged between 470 k counts/s and 602 k counts/s. However, at the higher excitation powers, the intensities of the emission show a non-linear increase and the rate of the increase in the emission counts decreases as shown in supporting information Figure S2 for two individual nanocubes. However, the Cu_2O nanocubes showed no saturation up to 207 μW average excitation power or 3.16E5 W/cm^2 excitation power density that means the emission of these nanocubes remains stable even with high laser excitation. The brightness of individual Cu_2O nanocubes suggests that a lower concentration of this nanomaterial might be required for biological imaging compared to the other fluorophores. Cytotoxicity of Cu_2O nanoparticles on fish blood has been studied which showed concentration lower than 8 $\mu\text{g}/\text{mL}$ has minor toxic effect for living cells²⁸. This is an important factor when considering that high concentrations of fluorophores can be toxic to a biological system²⁹.

Photostability of the Cu_2O nanocubes is also remarkable compared to standard commercially available fluorescent probes. It has previously been reported that commercially available fluorescent probes such as Alexa Fluor 647, polyacrylonitrile beads and carbon dots have a short bleaching time which limits their application for long

term bioimaging studies during the course of an experiment²¹. Photostability of Cu₂O was compared with photostability of Alexa 647, polyacrylonitrile beads, Au nanoclusters, carbon dots, nanodiamonds and nanorubies for two minutes²¹. Alexa 647 showed lowest photostability (2%) followed by Au nanoclusters (24%) and polyacrylonitrile beads (39%) (Fig. 4a and Table S1). Photostability of Cu₂O was the highest (100%) which is similar to nanodiamonds and nanorubies compared to the aforementioned fluorescent probes (Fig. 4a). This comparison further highlights the potential this material has for long term biological imaging applications. A bioimaging demonstration of the intrinsically fluorescent Cu₂O nanocubes was made through their use as fluorophores coupled with a mouse cumulus-oocyte complex. The Cu₂O nanocubes were imaged with the same experimental conditions used for optical characterization of individual and isolated nanocubes in Fig. 2. The fluorescence emission of the Cu₂O nanocubes was compared to the autofluorescence within the mouse cumulus-oocyte complex (Fig. 4b,c). The confocal image of the mouse cumulus-oocyte complex with Cu₂O nanocubes drop-casted on the surface is shown in Fig. 4b. The bright dots on the surface of the mouse cumulus-oocyte complex correspond to the fluorescence emission from Cu₂O nanocubes. The histogram in Fig. 4c shows the relative brightness of autofluorescence from the mouse cumulus-oocyte complex compared to Cu₂O nanocube fluorescence. The autofluorescence histogram collected from the distribution of pixel intensities within the boxed region in Fig. 4b and the Cu₂O histogram (Fig. 4c) shows the brightness distribution of 20 manually selected Cu₂O particles in Fig. 4b. Fluorescence from Cu₂O was observed to be four times higher in intensity compared to the autofluorescence signal from the cumulus-oocyte complex which made them easily distinguishable (Figs. 4c). The attractive characteristics of copper (I) oxide nanocubes, such as their long photostability and high brightness, highlight their potential as an alternative to commercially available fluorescent probes for bioimaging applications.

Conclusions

In conclusion, we have synthesised copper (I) oxide nanocubes via a seed-mediated method. Individual Cu₂O nanocubes were studied using a marked substrate which was milled with a focused ion beam to locate and collect optical data from 19 individual particles. This study reveals that single Cu₂O nanocubes can emit light at a rate of up to 487 K counts/s for at least 120 seconds with only 11 μW (1.7 W/cm²) laser excitation. Highly bright and photostable intrinsic fluorescence from copper (I) oxide nanocubes at low excitation powers suggest that the nanocubes are suitable for long time bioimaging experiments. Fluorescence from Cu₂O nanocubes was also observed to be significantly brighter than the auto-fluorescence from a fixed mouse cumulus-oocyte complex and highly photostable compared to commercially available organic fluorescent materials. However, for in vivo applications, there is further research to be undertaken to determine the biocompatibility of copper (I) oxide nanocubes as a function of their concentration in a biological context.

References

- Kuo, C. H., Chen, C. H. & Huang, M. H. Seed-Mediated Synthesis of Monodispersed Cu₂O Nanocubes with Five Different Size Ranges from 40 to 420 nm. *Advanced Functional Materials* **17**, 3773–3780, <https://doi.org/10.1002/adfm.200700356> (2007).
- Kuo, C.-H. & Huang, M. H. Morphologically controlled synthesis of Cu₂O nanocrystals and their properties. *Nano Today* **5**, 106–116 (2010).
- Kandjani, A. E. *et al.* Controlling core/shell formation of Nanocubic p-Cu₂O/n-ZnO toward enhanced photocatalytic performance. *Langmuir* **31**, 10922–10930, <https://doi.org/10.1021/acs.langmuir.5b01019> (2015).
- Zhang, J., Liu, J., Peng, Q., Wang, X. & Li, Y. Nearly Monodisperse Cu₂O and CuO Nanospheres: Preparation and Applications for Sensitive Gas Sensors. *Chemistry of Materials* **18**, 867–871, <https://doi.org/10.1021/cm052256f> (2006).
- Zoofakhar, A. S., Rani, R. A., Morfa, A. J., O'Mullane, A. P. & Kalantar-zadeh, K. Nanostructured copper oxide semiconductors: a perspective on materials, synthesis methods and applications. *J Mater Chem C* **2**, 5247–5270, <https://doi.org/10.1039/c4tc00345d> (2014).
- Gou, L. & Murphy, C. J. Solution-phase synthesis of Cu₂O nanocubes. *Nano Letters* **3**, 231–234 (2003).
- Park, J. C., Kim, J., Kwon, H. & Song, H. Gram-scale synthesis of Cu₂O nanocubes and subsequent oxidation to CuO hollow nanostructures for lithium-ion battery anode materials. *Advanced Materials* **21**, 803–807 (2009).
- Liu, R., Oba, F., Bohannan, E. W., Ernst, F. & Switzer, J. A. Shape control in epitaxial electrodeposition: Cu₂O nanocubes on InP (001). *Chemistry of materials* **15**, 4882–4885 (2003).
- Tsai, Y.-H., Chanda, K., Chu, Y.-T., Chiu, C.-Y. & Huang, M. H. Direct formation of small Cu₂O nanocubes, octahedra, and octapods for efficient synthesis of triazoles. *Nanoscale* **6**, 8704–8709 (2014).
- Chen, L. Y., Yu, J. S., Fujita, T. & Chen, M. W. Nanoporous copper with tunable nanoporosity for SERS applications. *Advanced Functional Materials* **19**, 1221–1226 (2009).
- Xu, L. *et al.* Solution-phase synthesis of single-crystal hollow Cu₂O spheres with nanoholes. *Nanotechnology* **17**, 1501 (2006).
- Ke, W. H., Hsia, C. F., Chen, Y. J. & Huang, M. H. Synthesis of Ultrasmall Cu₂O Nanocubes and Octahedra with Tunable Sizes for Facet-Dependent Optical Property Examination. *Small* **12**, 3530–3534 (2016).
- Yang, Z., Chiang, C.-K. & Chang, H.-T. Synthesis of fluorescent and photovoltaic Cu₂O nanocubes. *Nanotechnology* **19**, 025604 (2008).
- Serin, N. & Serin, T. The photocapacitance property of Cu/Cu₂O/Au sandwich structures. *Semiconductor science and technology* **17**, 1162 (2002).
- Qi, W. J., Huang, C. Z. & Chen, L. Q. Cuprous oxide nanospheres as probes for light scattering imaging analysis of live cells and for conformation identification of proteins. *Talanta* **80**, 1400–1405, <https://doi.org/10.1016/j.talanta.2009.09.042> (2010).
- Kondo, J. Cu₂O as a photocatalyst for overall water splitting under visible light irradiation. *Chemical Communications*, 357–358 (1998).
- Wu, S.-C., Tan, C.-S. & Huang, M. H. Strong Facet Effects on Interfacial Charge Transfer Revealed through the Examination of Photocatalytic Activities of Various Cu₂O-ZnO Heterostructures. *Advanced Functional Materials* **27**, 1604635, <https://doi.org/10.1002/adfm.201604635> (2017).
- Li, J. *et al.* Probing defects in nitrogen-doped Cu₂O. *Sci Rep* **4**, 7240, <https://doi.org/10.1038/srep07240> (2014).
- Kobayashi, H., Ogawa, M., Alford, R., Choyke, P. L. & Urano, Y. New strategies for fluorescent probe design in medical diagnostic imaging. *Chemical reviews* **110**, 2620–2640 (2009).
- Morfa, A. J. *et al.* Single-photon emission and quantum characterization of zinc oxide defects. *Nano Lett* **12**, 949–954, <https://doi.org/10.1021/nl204010e> (2012).
- Reineck, P. *et al.* Brightness and Photostability of Emerging Red and Near-IR Fluorescent Nanomaterials for Bioimaging. *Advanced Optical Materials* **4**, 1549–1557, <https://doi.org/10.1002/adom.201600212> (2016).

22. Jacques, S. L. Role of tissue optics and pulse duration on tissue effects during high-power laser irradiation. *Appl Opt* **32**, 2447–2454, <https://doi.org/10.1364/AO.32.002447> (1993).
23. Ampem-Lassen, E. *et al.* Nano-manipulation of diamond-based single photon sources. *Opt Express* **17**, 11287–11293 (2009).
24. Meczynska-Wielgosz, S., Piotrowska, A., Majkowska-Pilip, A., Bilewicz, A. & Kruszewski, M. Effect of Surface Functionalization on the Cellular Uptake and Toxicity of Nanozeolite A. *Nanoscale Res Lett* **11**, 123, <https://doi.org/10.1186/s11671-016-1334-8> (2016).
25. Chung, H. *et al.* The nuts and bolts of low-level laser (light) therapy. *Ann Biomed Eng* **40**, 516–533, <https://doi.org/10.1007/s10439-011-0454-7> (2012).
26. Goetz, M. *et al.* Near-infrared confocal imaging during mini-laparoscopy: a novel rigid endomicroscope with increased imaging plane depth. *J Hepatol* **53**, 84–90, <https://doi.org/10.1016/j.jhep.2010.01.039> (2010).
27. Foersch, S. *et al.* Confocal laser endomicroscopy for diagnosis and histomorphologic imaging of brain tumors *in vivo*. *PLoS One* **7**, e41760, <https://doi.org/10.1371/journal.pone.0041760> (2012).
28. Chen, L. Q., Kang, B. & Ling, J. Cytotoxicity of cuprous oxide nanoparticles to fish blood cells: hemolysis and internalization. *Journal of nanoparticle research* **15**, 1507 (2013).
29. Alford, R. *et al.* Toxicity of Organic Fluorophores Used in Molecular Imaging: Literature Review. *Molecular Imaging* **8**, 341–354, <https://doi.org/10.2310/7290.2009.00031> (2009).

Acknowledgements

N.Z. acknowledges RMIT University support of a PhD Scholarship. This work has been supported by ARC grants (FT110100225, LE140100131, CE140100003). B.C.G. acknowledges the support of an ARC Future Fellowship (FT110100225). Experiments were performed in the ARC Centre of Excellence for Nanoscale BioPhotonics (CNBP) laboratories and the RMIT Microscopy and Microanalysis Facility (RMMF) at RMIT University. CNBP and RMMF technical staffs are acknowledged for their help and assistance with setting up the experiments.

Author Contributions

N.Z. carried out the experiments. N.Z., A.E.K., A.O., M.R.H. and B.C.G. analysed the data, contributed to data interpretation. H.M.B. provided the mouse cumulus-oocyte complexes. All authors contributed in the manuscript writing. B.C.G. supervised the research.

Additional Information

Supplementary information accompanies this paper at <https://doi.org/10.1038/s41598-017-17295-0>.

Competing Interests: The authors declare that they have no competing interests.

Publisher's note: Springer Nature remains neutral with regard to jurisdictional claims in published maps and institutional affiliations.



Open Access This article is licensed under a Creative Commons Attribution 4.0 International License, which permits use, sharing, adaptation, distribution and reproduction in any medium or format, as long as you give appropriate credit to the original author(s) and the source, provide a link to the Creative Commons license, and indicate if changes were made. The images or other third party material in this article are included in the article's Creative Commons license, unless indicated otherwise in a credit line to the material. If material is not included in the article's Creative Commons license and your intended use is not permitted by statutory regulation or exceeds the permitted use, you will need to obtain permission directly from the copyright holder. To view a copy of this license, visit <http://creativecommons.org/licenses/by/4.0/>.

© The Author(s) 2017